Supporting Information for

Interconnected Carbon Nanosheets Derived from Hemp for Ultrafast Supercapacitors with High Energy

Huanlei Wang, [†,‡] Zhanwei Xu, [†,‡] Alireza Kohandehghan, [†,‡] Zhi Li, [†,‡,*] Kai Cui, [‡] Xuehai Tan, [†,‡] Tyler James Stephenson, [†,‡] Cecil K. King'ondu, [†,‡] Chris M. B. Holt, [†,‡] Brian C. Olsen, [†,‡] Jin Kwon Tak, [§] Don Harfield, [§] Anthony O. Anyia, [§] and David Mitlin, [†,‡,*]

[†] Chemical and Materials Engineering, University of Alberta, Edmonton, Alberta T6G 2V4, Canada

[‡] National Institute for Nanotechnology (NINT), National Research Council of Canada, Edmonton, Alberta T6G 2M9, Canada

[§] Bioresource Technologies, Alberta Innovates - Technology Futures, Vegreville, Alberta, T9C 1T4, Canada

*Address correspondence to lizhicn@gmail.com (L. Zhi); dmitlin@ualberta.ca (D. Mitlin).

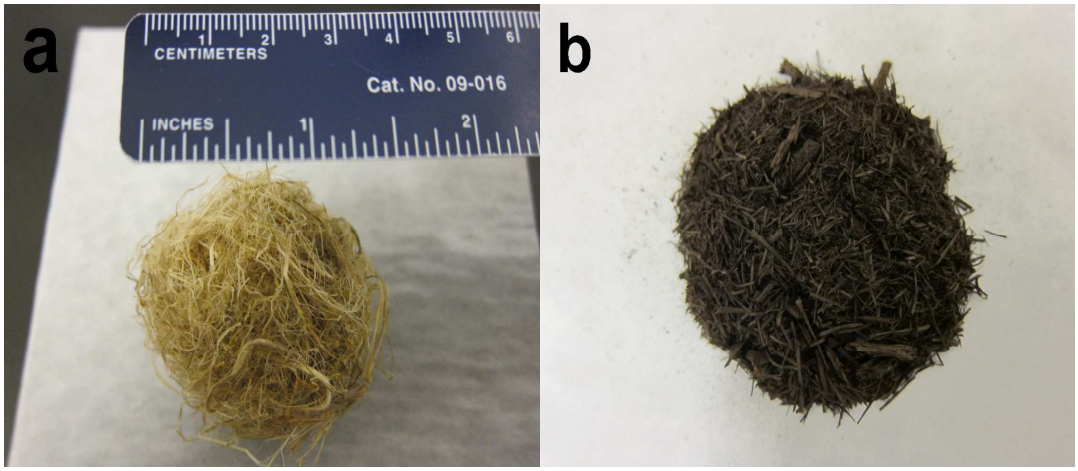

Figure S1. Photographic images of hemp bast fiber (a) before and (b) after hydrothermal carbonization.

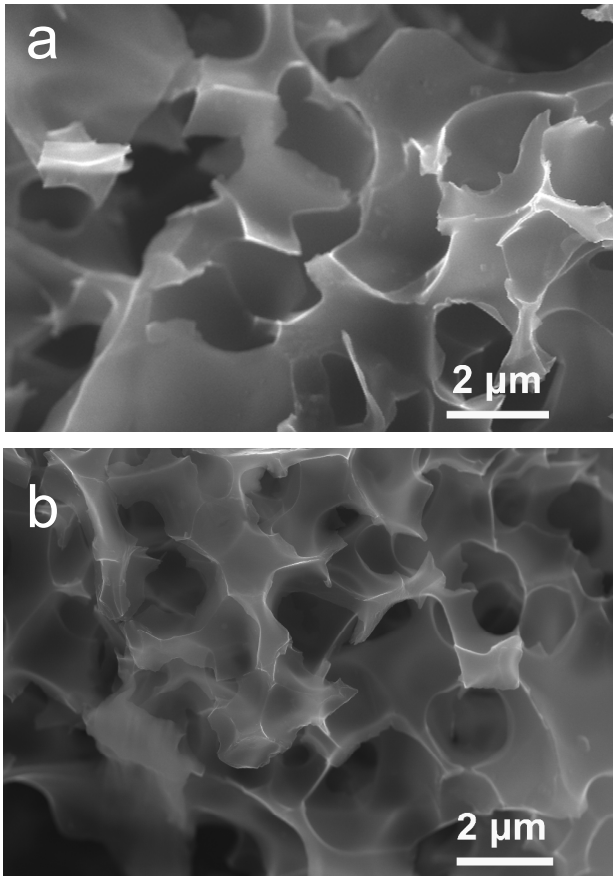

Figure S2. SEM images of (a) CNS-700 and (b) CNS-750.

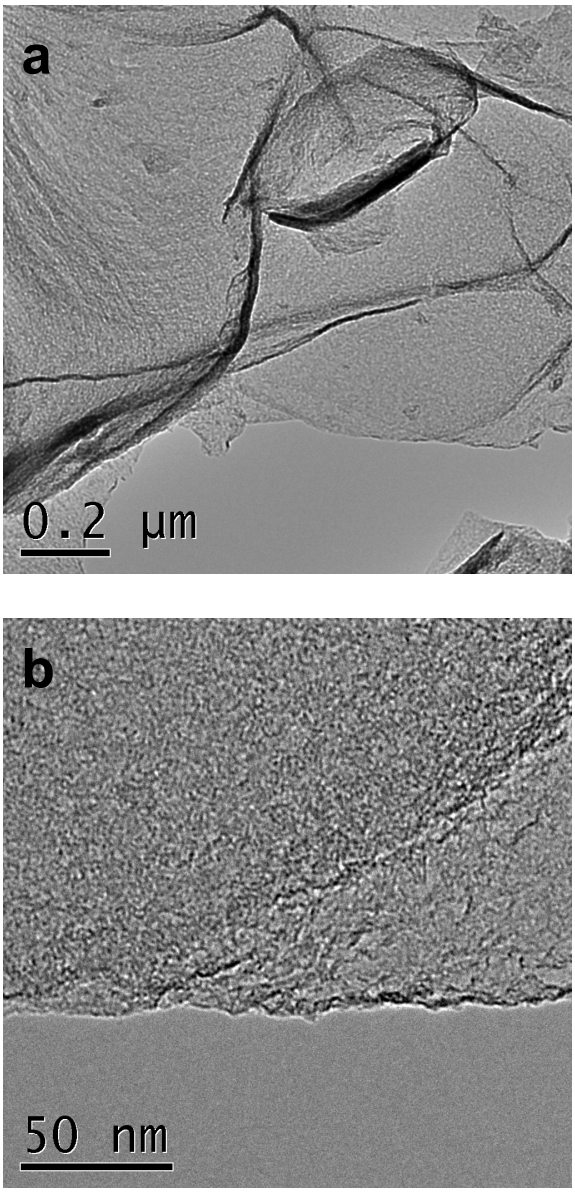

Figure S3. TEM images of sample CNS-800.

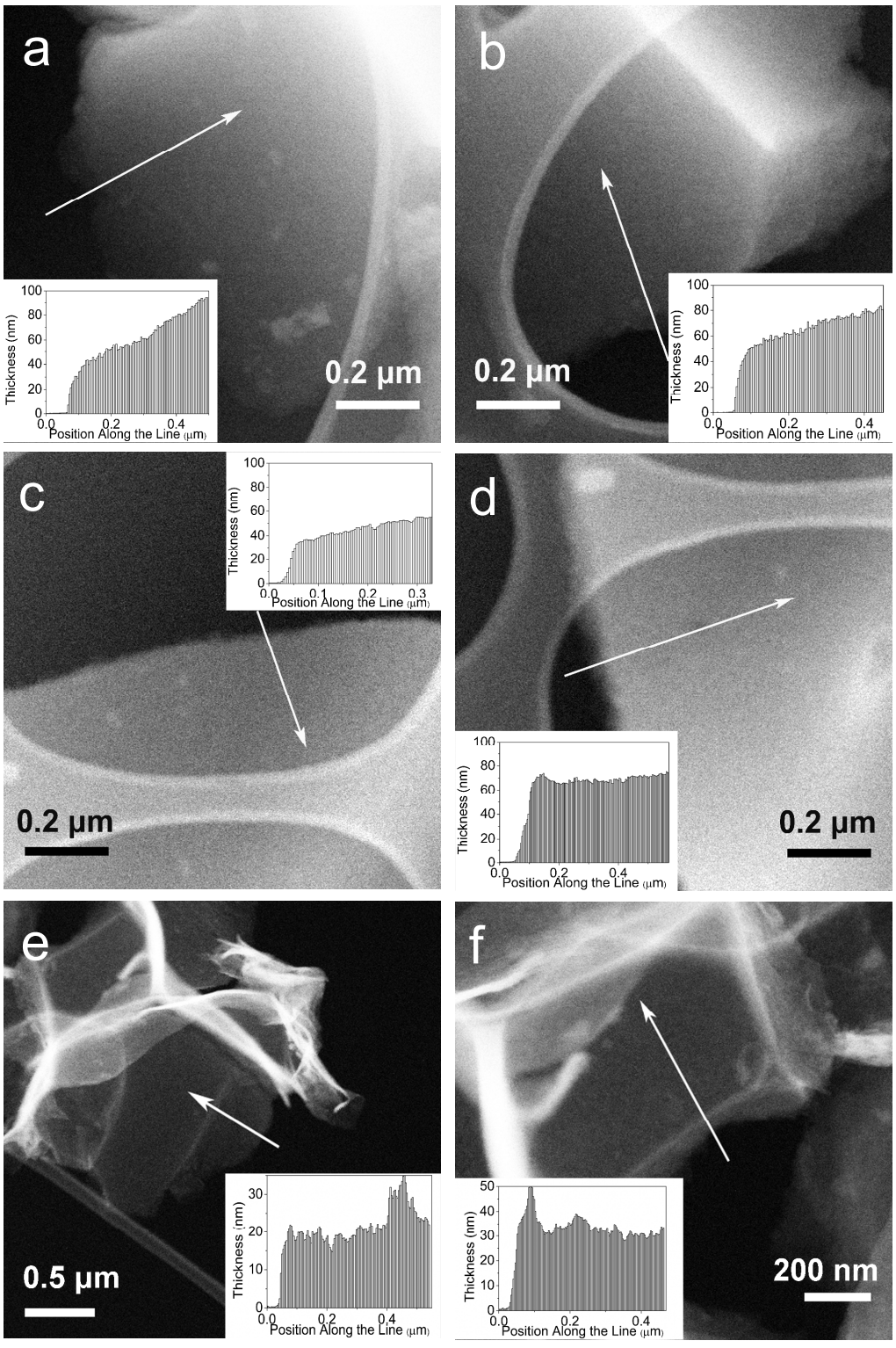

Figure S4. Annual dark-field images and EELS thickness curves (inset) of (a,b) CNS-700, (c,d) CNS-750 and (e,f) CNS-800.

Table S1. Carbon, oxygen, and nitrogen contents in the studied samples obtained from X-ray photoelectron spectroscopy

Samples	C_{XPS} (at%)	N_{XPS} (at%)	O_{XPS} (at%)
biochar	73.54	1.77	24.69
CNS-700	93.69	0.90	5.41
CNS-750	93.39	1.01	5.60
CNS-800	94.33	1.48	4.19
AC	95.35	-	4.65
CG	93.97	-	6.03

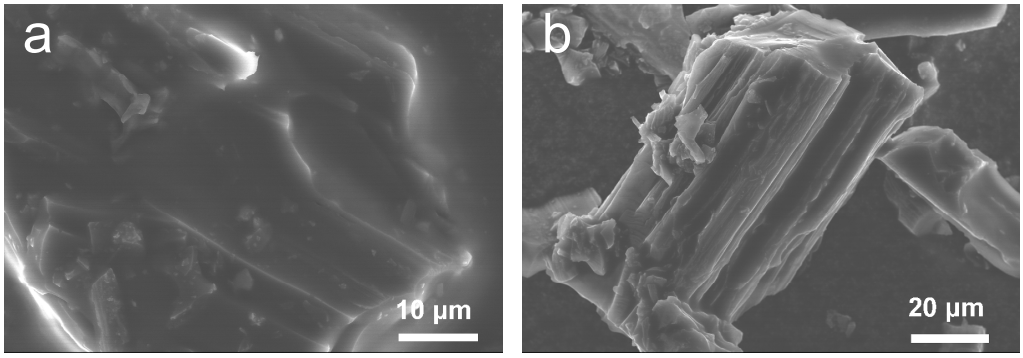

Figure S5. (a) SEM micrograph of the carbon material obtained by direct carbonization of hemp bast fiber. (b) SEM micrograph of the specimen after KOH activation.

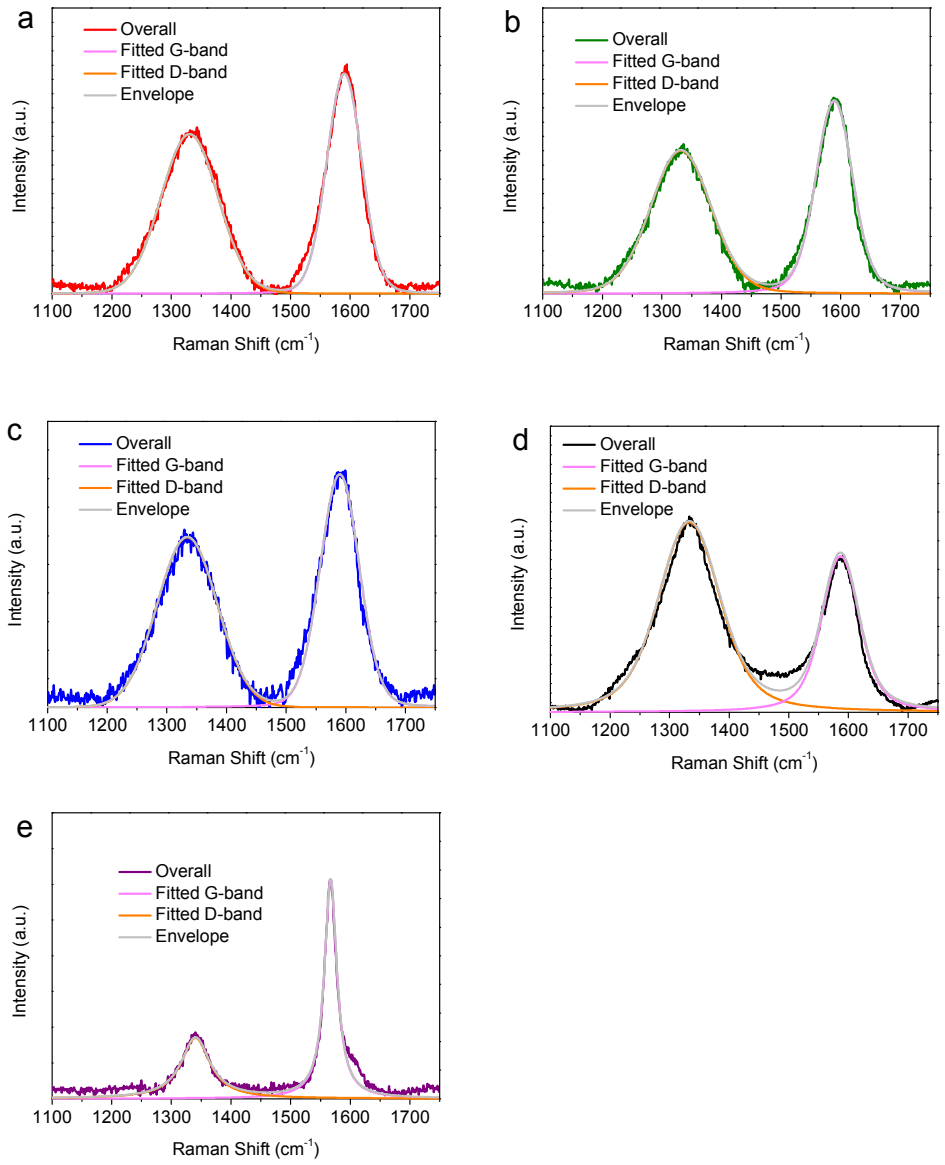

Figure S6. Raman spectra and fitted Raman curve of (a) CNS-700, (b) CNS-750, (c) CNS-800, (d) AC, and (e) CG. (For simplicity, a two-symmetric-line fit (D and G bands) using a Voigt function was applied to describe the Raman curves.[1])

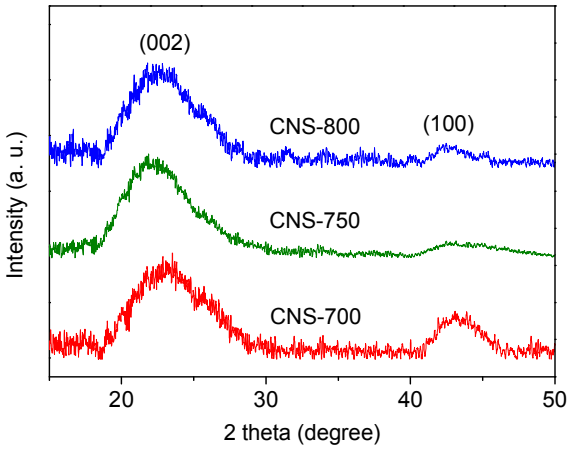

Figure S7. XRD patterns of the resultant carbon nanosheets.

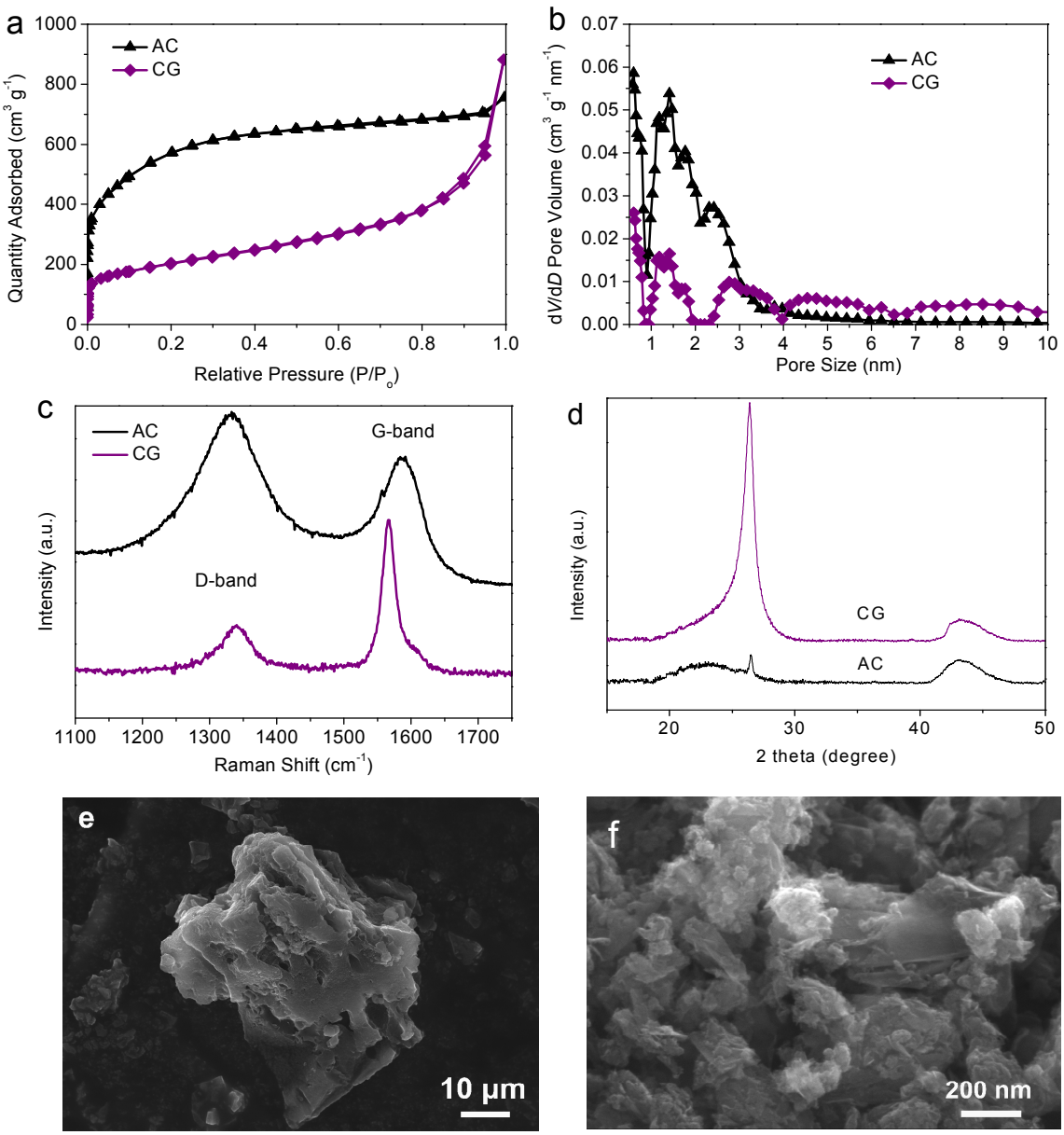

Figure S8. (a) Nitrogen adsorption-desorption isotherms of commercial activated carbon (AC), commercial graphene nanoplatelets (CG). (b) Pore size distributions calculated from nitrogen adsorption isotherms using the DFT method. (c) Raman spectra of baseline AC and CG. (d) XRD patterns of AC and CG. SEM micrographs of (e) AC and (f) CG.

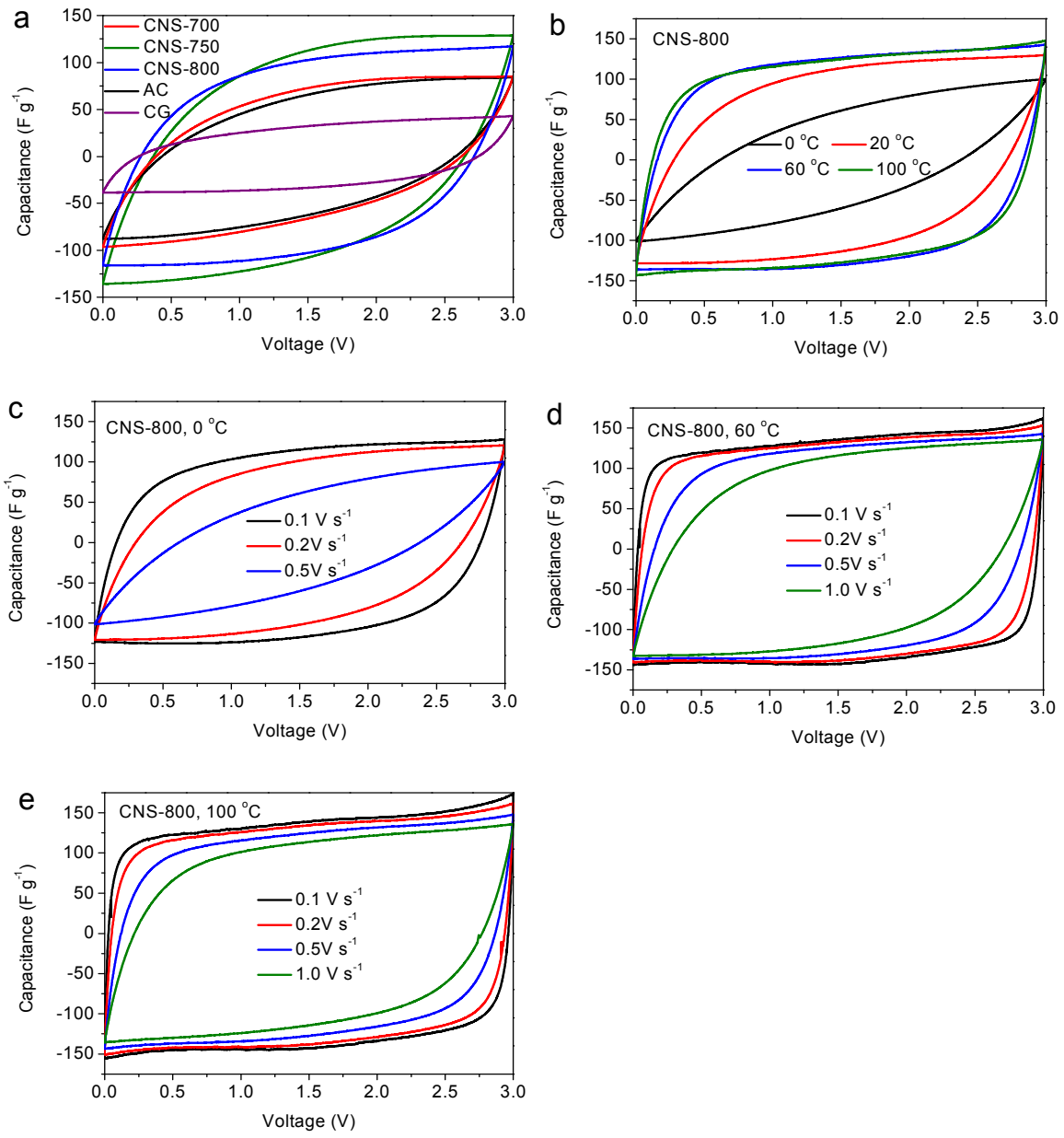

Figure S9. (a) CV curves of resultant carbon nanosheets, commercial activated carbon and commercial graphene nanoplatelets measured at 20 °C and 500 mV s^{-1}. (b) CV curves of CNS-800 tested at different temperatures using a scan rate of 500 mV s^{-1}. (c) CV curves of CNS-800 at scan rates from 0.1 to 0.5 V s^{-1}, tested at 0°C. (d) CV curves of CNS-800 at scan rates from 0.1 to 1 V s^{-1}, tested at 60 °C. (e) CV curves of CNS-800 at scan rates from 0.1 to 1 V s^{-1}, tested at 100 °C.

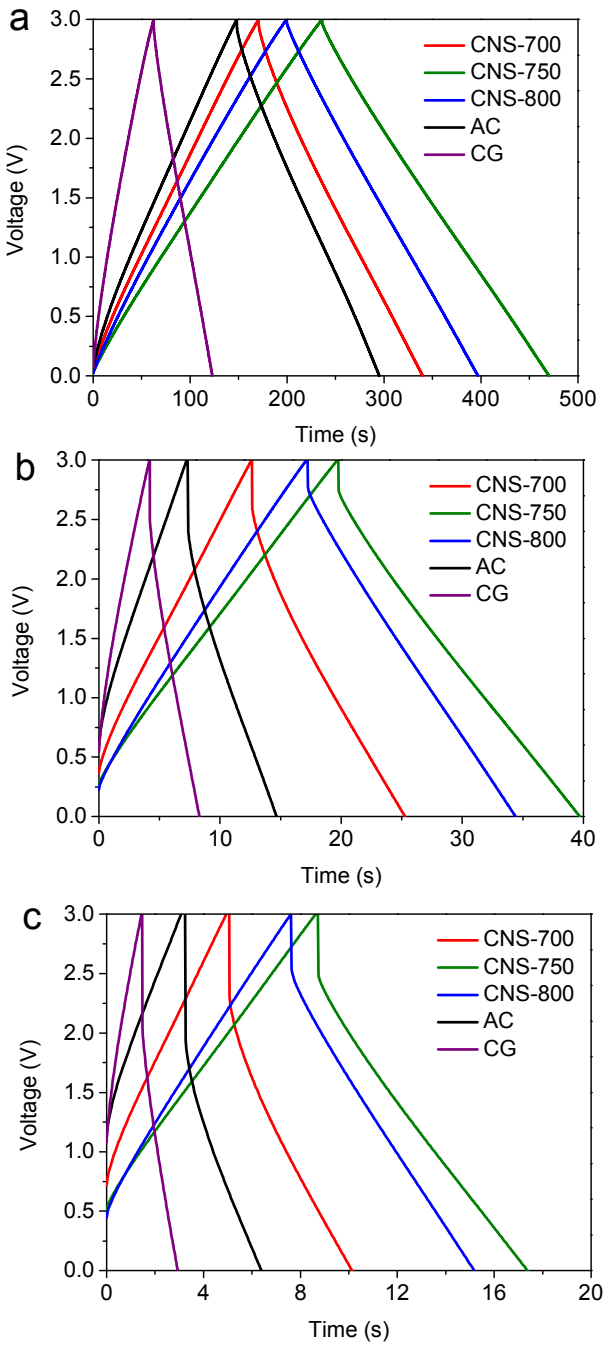

Figure S10. Galvanostatic charge-discharge profiles of carbon nanosheets, commercial activated carbon and commercial graphene nanoplatelets at current densities of (a) 1, (b) 10 and (c) 20 A g^{-1}, tested at 20 °C.

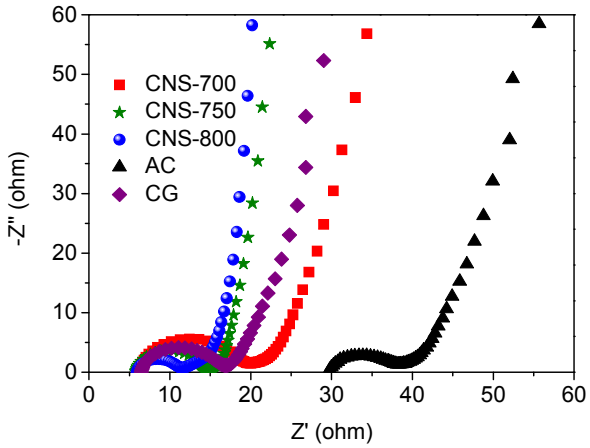

Figure S11. Nyquist plots comparing carbon nanosheets, commercial activated carbon and commercial graphene nanoplatelets, measured at 20 °C.

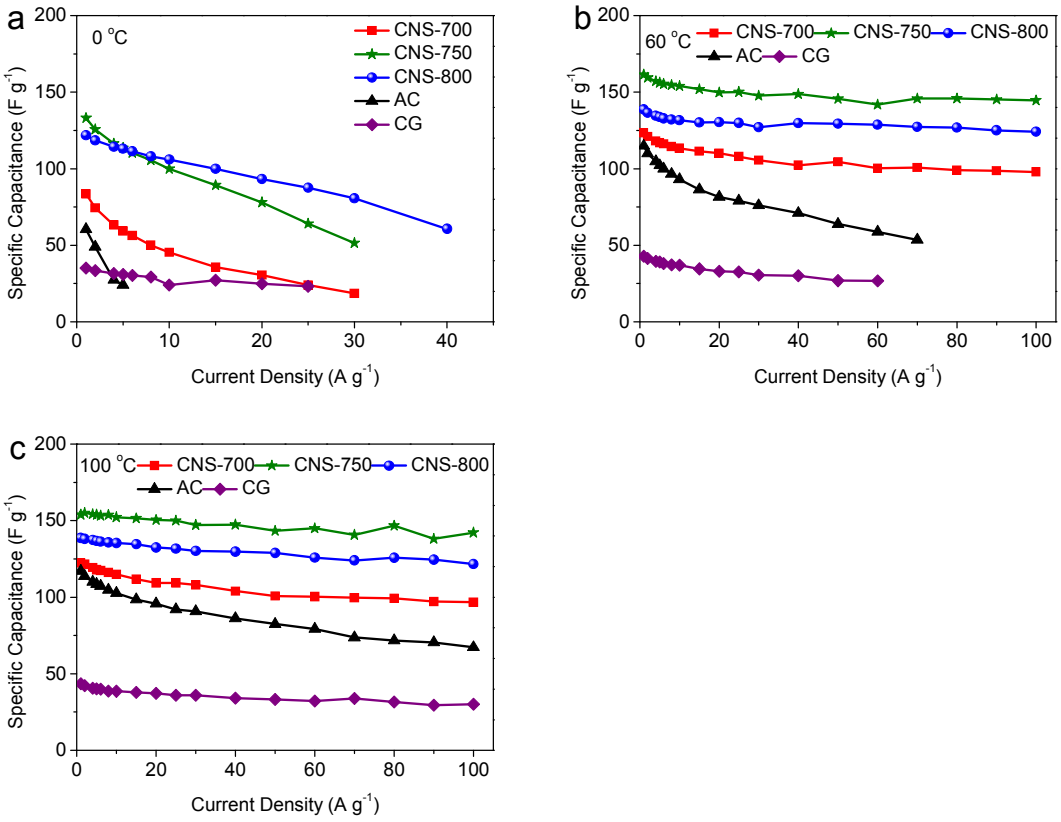

Figure S12. Specific capacitance *versus* current density, tested at (a) 0 °C, (b) 60 °C, and (c) 100 °C.

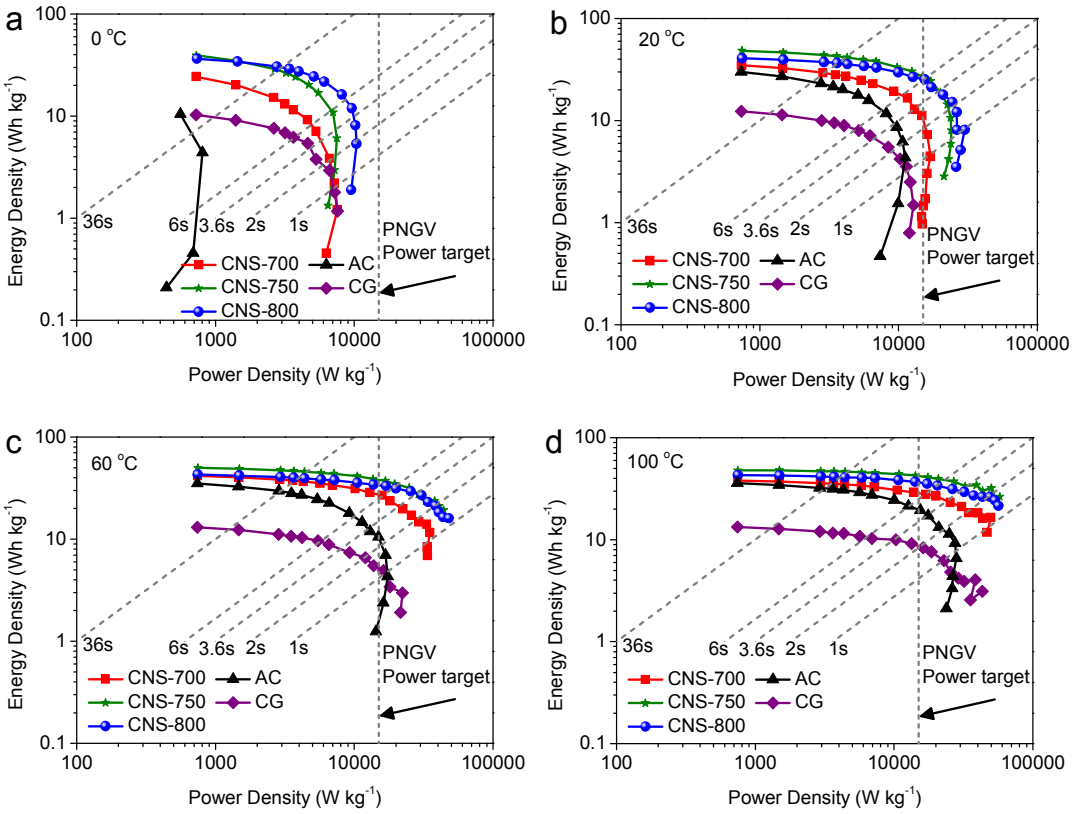

Figure S13. Ragone Charts based on active materials comparing carbon nanosheets, commercial activated carbon and commercial graphene nanoplatelets, evaluated at (a) 0 °C, (b) 20 °C, (c) 60 °C, and (d) 100 °C.

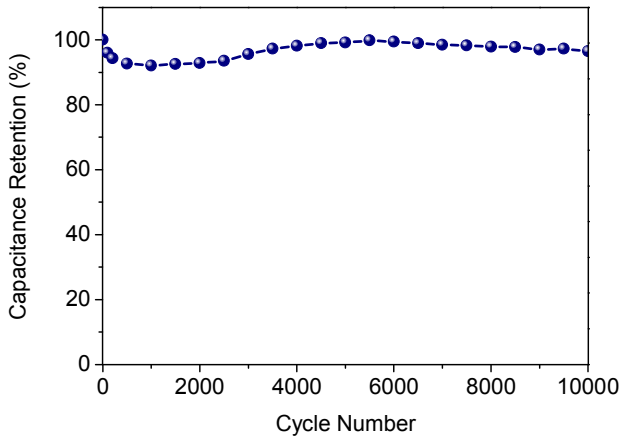

Figure S14. Capacitance retention *versus* the cycle number for CNS-800, measured at 10 A g^{-1} and 60 °C.

REFERENCES AND NOTES

1. Zickler, G. A.; Smarsly, B.; Gierlinger, N.; Peterlik, H.; Paris, O. A Reconsideration of the Relationship between the Crystalline Size L_a of Carbons Determined by X-Ray Diffraction and Raman Spectroscopy. *Carbon* **2006**, *44*, 3239-3246.